DOI 10.1007/s10812-020-01098-9
Journal of Applied Spectroscopy, Vol. 87, No. 5, November, 2020 (Russian Original Vol. 87, No. 5, September–October, 2020)

DETECTION OF ETHYLENEDIAMINE VAPOR BY OPTICAL WAVEGUIDE SENSOR BASED ON TETRAKIS-CARBOXYLPHENYL PORPHYRIN FILM

Qingrong Ma, Yuan Zhang, Hannikezi Abudukeremu, Asiya Maimaiti, Kediliya Wumaier, Patima Nizamidin, and Abliz Yimit *

UDC 547.415.1

A sensitive element was prepared by the spin coating method on the surface of a K^+ exchange glass optical waveguide by dissolving tetrakis-carboxyphenyl porphyrin (TCPP) in the nontoxic solvent ethanol. The TCPP sensitive element detected 18 volatile organic compounds with an excellent selective response to ethylenediamine (EDA) gas. On this basis, the effects of the solvent, solution mass fraction, speed of the homogenizer and atmospheric humidity on the detection of EDA gas by the sensitive element were discussed. The formation of hydrogen bonds between TCPP and EDA molecules is proposed, which leads to changes in the morphology and light absorbance of the sensing film.

Keywords: *tetrakis-carboxylphenyl porphyrin, optical waveguide sensor, volatile organic compounds, ethylenediamine.*

Introduction. China's national economy has shown rapid development, and the rate of industrialization is staggering. However, these advances have also resulted in many environmental problems to which the government are paying close attention. Volatile organic compounds (VOCs), which are typically toxic, explosive, flammable, and environmentally hazardous, are extensively used in R&D laboratories and industrial production [1]. Among these hazardous gases, amine complexes are commonly used in agriculture, pharmaceuticals, and the dye manufacturing and food processing industries, and these complexes are toxic, irritants, and corrosive to human skin, eyes, and the respiratory system [2]. Lv et al. [3] studied the effects of ethylenediamine (EDA) on the workers of Harbin Aircraft Manufacturing Company. EDA was initially observed in the nervous system, respiratory system, and immune system, and was shown to be neurotoxic and cause irritation and sensitization. When the concentration of EDA is within the range of 4–1000 mg/m^3, a series of neurological symptoms can occur upon exposure. Wang et al. [4] conducted on-site sampling and detected EDA gas in accordance with standards such as the "sampling specifications for monitoring hazardous substances in workplace air." Tan et al. [5] identified the occupational-disease-inductive factors of EDA, xylene, and other gases produced in an auxiliary refinery production plant, analyzed and evaluated them to determine the key points, and tested for occupational-disease-inductive protection. These investigations require many samples and complex sample processing but also need a testing of staff members. Therefore, it is of great significance to strengthen the prevention and treatment of the occupational hazards of EDA, especially the fabrication of a simple, rapid, effective, and low cost sensor. The optical waveguide (OWG) sensing method is a promising approach for tracing gaseous pollutants at a low concentration level (ppm or ppb) owing to its high sensitivity, fast response, anti-electromagnetic interference, simple and safe operation, and low production cost [6].

Owing to its extraordinary electron transfer and photoluminescence properties, porphyrin molecules are quite stable, and their properties can be precisely tuned by modifications of their molecular structure [7]. Therefore, they have been used in biochemistry, medicine (enzymes [8], photodynamic therapy), analytical chemistry and synthesis, and materials science. Porphyrins in gas sensor research have resulted in innumerable achievements [9–12].

We seek to develop a tetrakis-carboxyphenyl porphyrin (TCPP) OWG gas sensor that is easy to prepare and operate. It is to be used to detect the concentration of EDA in a factory in real time to help reduce the harm of EDA to the health of workers.

*To whom correspondence should be addressed.

College of Chemistry and Chemical Engineering, Xinjiang University, Urumqi 830046, China; email: ablizy@sina.com. Abstract of article is published in Zhurnal Prikladnoi Spektroskopii, Vol. 87, No. 5, p. 856, September–October, 2020.

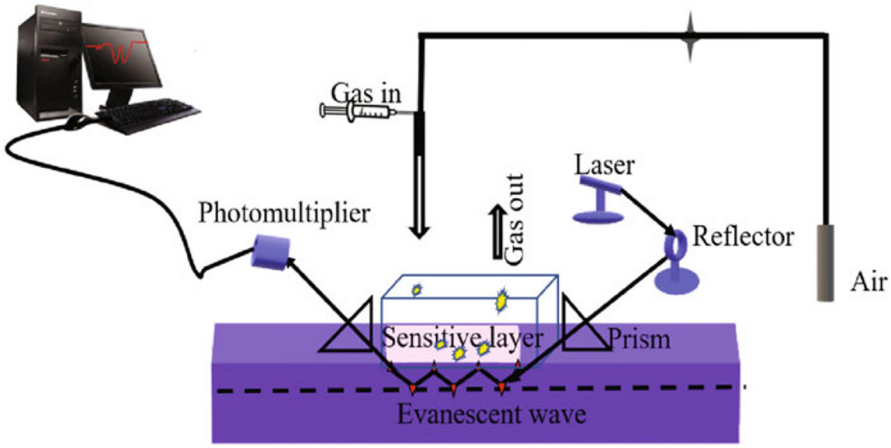

76 × 26 × 1 mm

Fig. 1. OWG detection system.

Experimental. *Reagents and instruments*. Ethanol and chloroform were laboratory grade and purchased from Tianjin Zhiyuan Chemical Reagent Co. Ltd. TCPP was laboratory grade and purchased from Shanghai Mineral Chemical Technology Co. Ltd.

Samples were analyzed using field emission scanning electron microscopy (SEM, SU8019 microscope, Japan Hitachi Company); UV-vis spectrophotometry (UV-vis, Uv-1780, Japan); and Fourier-transform infrared spectroscopy (FT-IR, FT-IR-650, China). A vacuum drying chamber (DHG-9023A, Shanghai, China), spin coater (KW-4A, Shanghai, China), humidometer (AS 847, Dongguan, China), gas detection tube (working range: 2–200 ppm, Beijing, China), and OWG testing systems (self-assembled in our laboratory) were used.

Preparation of VOCs and K^+ exchange OWG film. VOCs were prepared by the natural drying method in our laboratory, where certain organic liquids with a measured concentration were injected into a 600-mL bottle by a microsyringe and left to stand for 3 h. A certain amount of KNO_3 powder was heated in a muffle furnace. After melting, an ordinary glass slide (76 × 26 × 1 mm) was immersed. and the temperature was kept at 400^{o}C for 40 min. A K^+ exchange glass OWG element was obtained by washing with distilled water and setting aside to cool.

Different humidity of water vapor configuration method. The relative humidity of a saturated salt solution can create a stable moist atmosphere [13, 14], which is a common standard. This standard is widely used, simple to install, and facilitates good moisture reappearance. The saturated salt static humidity generator used in our work was homemade.

Testing system. An OWG gas sensor is mainly dependent on the evanescent wave principle [15]. The fundamental components (Fig. 1) comprise a semiconductor laser, photomultiplier, K^+ exchange glass substrate, sensing materials, a pair of prisms (*ns* = 1.75), and a computer. Generally, we choose a higher refractive index light-sensitive material that can be immobilized on the substrate surface in some way. When the sensing element was installed in the testing system, a certain wavelength from a semiconductor laser beam propagated through one prism. When the incident angle of the input light satisfied the special incidence angle, the light was totally reflected and propagated in the guided wave layer. In the process of propagation, light is in the form of propagating evanescent waves and can be accessed in the sensing film in the guided wave layer. When the sensing film and gas interact, the output light intensity will change, which is registered by the computer.

Results and Discussion. *Selection of light source*. To select the light source of the OWG, we measured the absorbance of the thin film before and after exposure to VOCs by UV-vis spectrophotometry. Figure 2 shows that a well-defined Soret band was observed for TCPP at 419 nm, owing to the π–π^* transition of the porphyrin ring, and four *Q* bands at 514, 548, 589, and 645 nm [16], which was the same as the TCPP film. This showed that no J or H type aggregation behavior [17, 18] took place on the K^+ exchange glass OWG element. For the TCPP thin film exposed to EDA gas, the absorbance exhibited a larger increase than before exposure under 420 nm, which can improve the sensitivity of the sensitive film in the OWG test. However, for the laser light at λ = 420 nm, because the wavelength is short and the light intensity is weak, a weak light absorbance is observed. Therefore, based on the above analysis, the laser light at λ = 520 nm was selected as the detection light source of the OWG system to detect the EDA analyte.

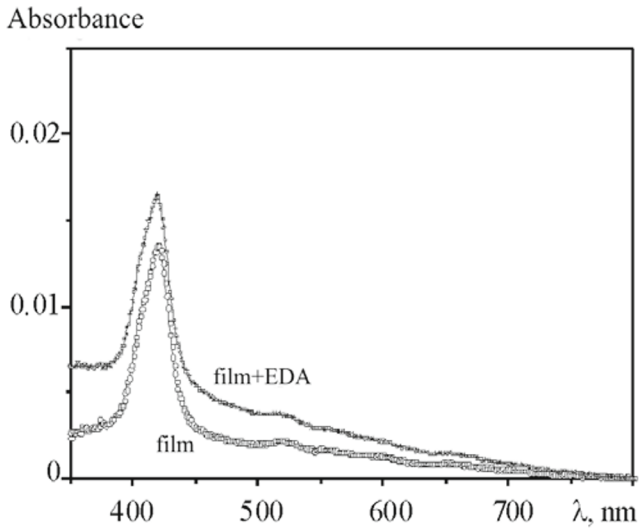

Fig. 2. UV-vis spectra of TCPP film before and after contacting with EDA gas.

Optimization of preparation conditions for sensitive elements. The TCPP film was adhered to glass by spin coating, and there were two factors to consider. First, different types of solvent have different effects on the solute owing to the polarity of the solution. Second, the volatility and surface tension of the solvents have an influence on forming thin films by means of the spin coating method. TCPP is a kind of polar organic material that requires the choice of a corresponding polar solvent. When TCPP dissolves in DMF, it exhibits a large solubility, but the volatility of solvents is low over a short time, which results in an imperfect TCPP film. Ethanol has a large polarity, volatility, and low surface tension; therefore, a TCPP film can be successfully fabricated by the spin coating method.

In OWG sensors, the film thickness may affect the sensing performance of the OWG element. The surface sensitivity of the thin-film optical waveguide is defined by the following formula [19]:

$$S_{\mathrm{OWG}} = \left(\frac{n_{\mathrm{surf}}^2}{2N_{\mathrm{eff}}}\right)\frac{E_y(0)^2}{\int_{-\infty}^{+\infty} E_y(x)^2\,dx},$$

where S_{OWG} is the surface sensitivity of the thin-film optical waveguide; n_{surf} is the average surface refractive index defined by $(n_f + n_c)^{1/2}$, where the refractive index of the thin-film optical waveguide is given as n_f and that of the cladding layer is n_c; N_{eff} is the effective refractive index of the waveguide; $E_y(x)$ refers to the electric field distribution of the guided light, namely, the mode of optical waves, and, in this case, mainly shows the TE_0 mode, and $E_y(0)$ is the intensity of the electric field on the surface of the optical waveguides. As is clearly shown in the formula for the surface sensitivity, the sensitivity is related to the refractive index and cut-off thickness of the thin-film OWG.

Gas exposure. Furthermore, the TCPP film was immobilized on the OWG testing system and then exposed to 18 different kinds of VOCs with the same concentration of 1000 ppm. The output light intensity changed by the following equation [20]: $\Delta I = I_{\mathrm{gas}} - I_{\mathrm{air}}$ (where I_{gas} is output light intensity in the gas and I_{air} is the output light intensity in the surrounding air). As is shown in Fig. 3a–e, the TCPP film under different conditions presented various responses to the selected analytes, among which the sensing element with a mass percentage of 0.08% and a rotating speed of 1500 rpm exhibited the best response to the EDA vapor gas. Here, we performed the SEM characterization of the TCPP film under optimal conditions and found that TCPP appeared to self-assemble into a dense, well-dispersed monolayer on the glass surface, where the particle size was estimated to be approximately 10.65 nm, but ranged from 8.45 to 15.86 nm (Fig. 4a), and the thin film thickness was approximately 75 nm (Fig. 4b), which led to the good adsorbability for gas molecules.

Figure 5a shows the response curve obtained under the best conditions. The output light intensity decreased when the sensitive film was exposed to the gas analytes, and this process was the response time. As the gas analytes were moved from the flow cell with the carrier gas, the output light intensity recovered to its initial state; this process was the recovery time. The signal change of EDA (ΔI = 720) possessed a greater response, where the response time was approximately 5 s and the

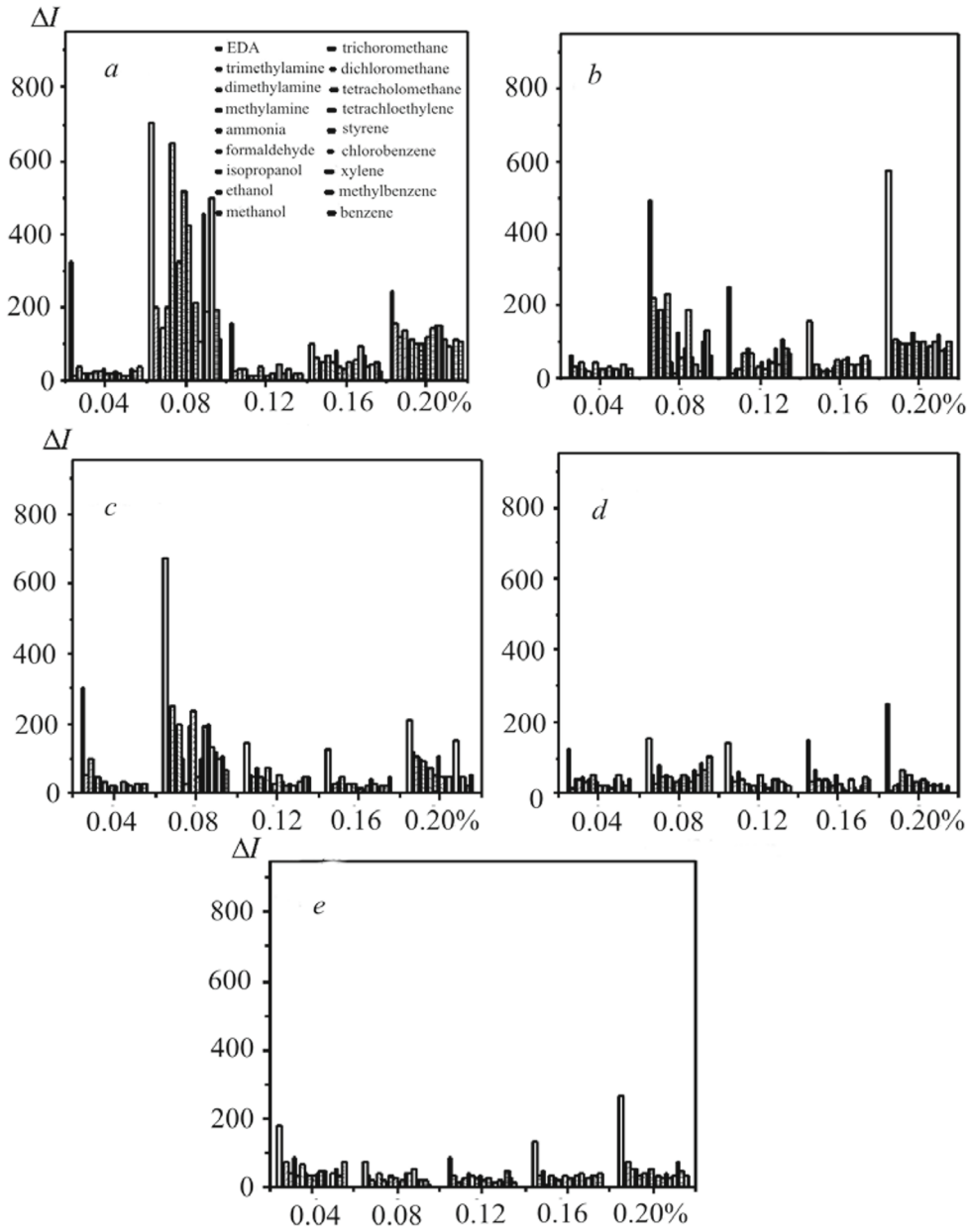

Fig. 3. Histograms of the TCPP-based K^+ exchange glass film OWG device prepared with rotating speeds of 900 (a), 1200 (b), 1500 (c), 1800 (d), and 2100 rpm (e), where the films were developed from a porphyrin solution with mass fractions of 0.04, 0.08, 0.1, 0.14, and 0.18%.

recovery time was 10 s. Meanwhile, we determined the reproducibility of the experiment with 1000 ppm EDA, as shown in Fig. 5b, where EDA had an effective stability with the RSD = 4.9%.

Relative humidity effect. The effect of atmospheric humidity on the experiment cannot be underestimated. The TCPP sensor was exposed to different humidity atmospheres in the range from 20–95% and 1000 ppm cross atmosphere. It can be seen from Fig. 6a that as the RH was increased from 20 to 75%, the output light intensity of the gas sensor slightly increased for EDA at the same concentration, which may arise from the increased intermolecular force between water molecules and EDA, which increased the energy of the whole system, thus increasing the output light intensity. However, in the process of the experiment, the influence of the 95% environmental humidity on the sensitive components cannot be ignored. Its recovery time was long, which may be caused by the interaction between a hydrophilic carboxyl group and hydroxyl group on the

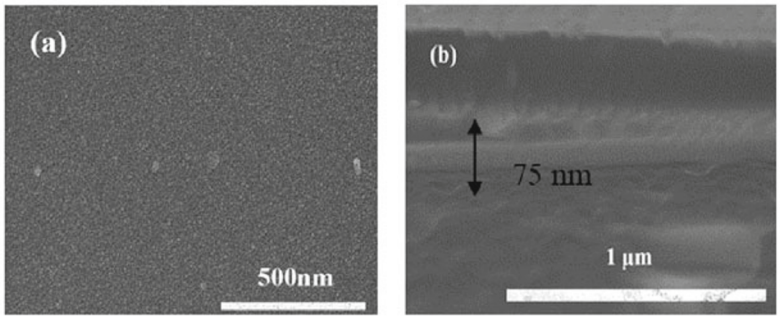

Fig. 4. (a) FESEM image of the TCPP film; (b) FESEM image of TCPP film cut-off area thickness.

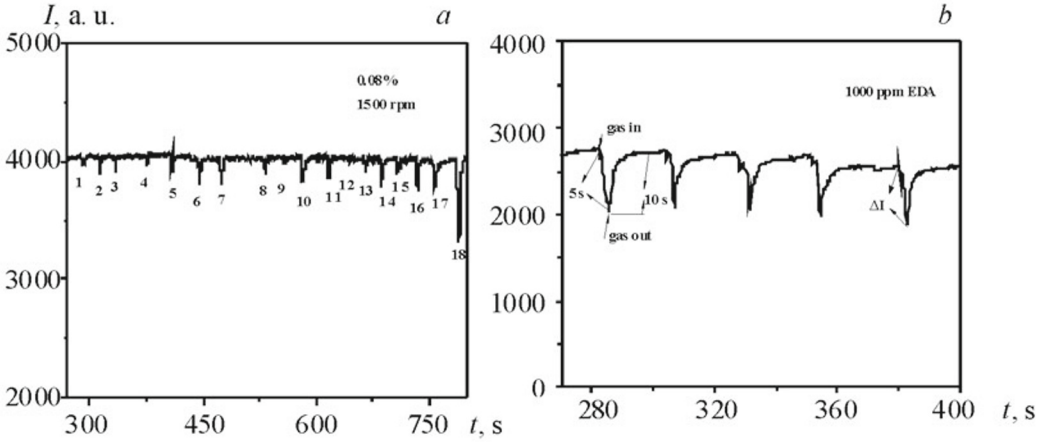

Fig. 5. a) Dynamic response curve of the TCPP sensor to 1000 ppm of gas analytes (18 VOCs: 1) benzene, 2) methylbenzene, 3) xylene, 4) chlorobenzene, 5) styrene, 6) tetrachloroethylene, 7) trichloromethane, 8) tetrachloromethane, 9) dichloromethane, 10) methanol, 11) isopropanol, 12) ethanol, 13) formaldehyde, 14) ammonia, 15) methylamine, 16) dimethylamine, 17) trimethylamine, 18) EDA); b) reproducibility experiment with 1000 ppm EDA.

surface. Meanwhile, the error bar graph (n = 5) of the parallel experiment is shown in Fig. 6b, where the difference was not significant.

EDA Gas Low-Concentration Test. After investigating the influence of the above factors on the sensor, we conducted the EDA low-concentration test under the condition of 1500 rpm and 0.08% mass fraction at room temperature. The study found that the sensor was able to detect 0.1 ppm (S/N = 5.05; Fig. 7a). To ensure the accuracy of the sensor for detecting EDA gas, multiple parallel experiments were conducted. The Y-axis error line graph was obtained by using the standard deviation as the Y-axis error as shown in Fig. 7b. The linear relationship between the average values of the parallel experiments was good, and the linear equation was $\log \Delta I = (3.62103 \pm 0.14438) + (0.2539 \pm 0.03254) \log C$, $R^2 = 0.9850$, S/N = 5.05, and RSD = 6.25%, which indicated that the sensor exhibits a good repeatability in response to the EDA gas.

Investigation of the Mechanism. The absorption of light causes the properties of porphyrin molecules to change greatly in the electronic excitation state, such as dipole moment, hydrogen bond capacity, and ion dissociation constant [21]. From the experimental results, the charge transfer process in the form of a hydrogen bond is the most likely mechanism for this behavior [22, 23]. Porphyrins maintain a certain energy difference between the highest and lowest occupied molecular orbitals, that is, porphyrins exhibit π–π electron transitions when laser light passes through the glass waveguide, which may arise from electron transitions on N atoms to vacancies in the porphyrin ring. Owing to this change in the distribution of

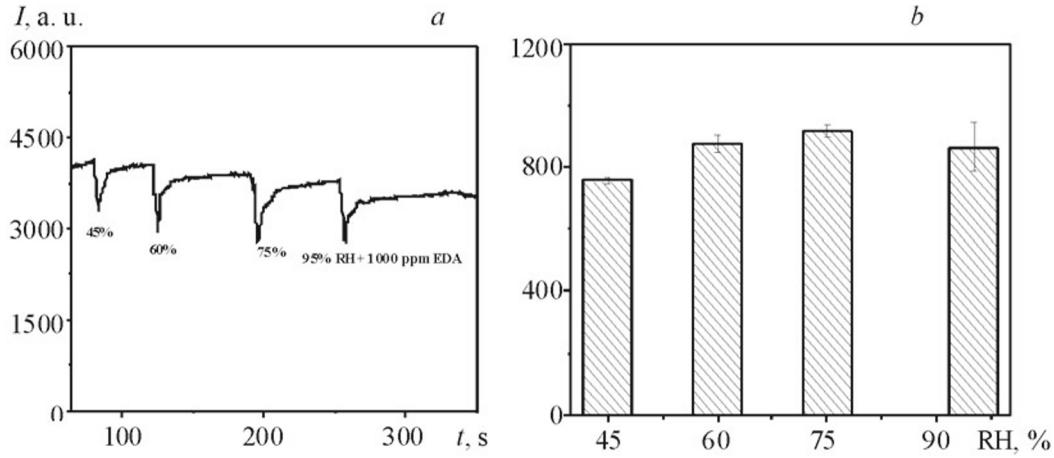

Fig. 6. a) Dynamic response curve of the TCPP sensor to 1000 ppm of EDA gas analytes in different moisture atmospheres; b) error bar graph.

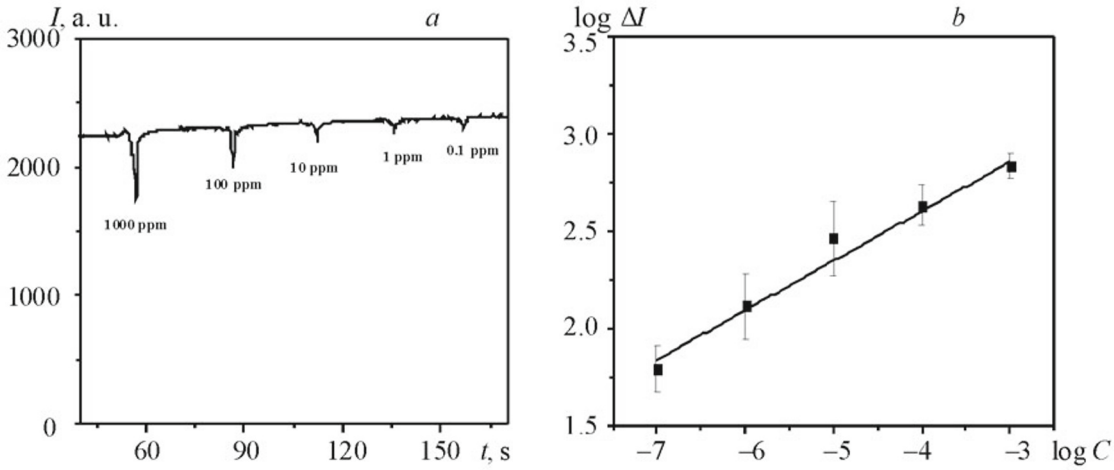

Fig. 7. a) Spectrum of sensitive film in response to a low concentration of EDA; b) the linear relationship between the concentration of gas and the standard deviation.

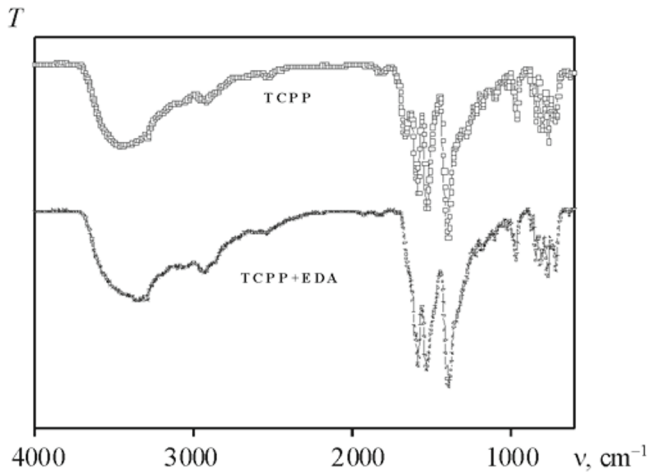

Fig. 8. FT-IR spectra of TCPP film and the film after contacting with EDA gas.

electrons, protons behave differently in the excited state; therefore, the distance between the donor (EDA) and the acceptor (TCPP), the relative position of the proton in the hydrogen bond, and the energy difference between the two energy levels of the porphyrin molecule are different when an EDA molecule interacts with the sensitive membrane [24, 25].

Figure 8 shows the FT-IR spectra of TCPP and TCPP interacting with EDA, where the TCPP peak showed a stretching vibration of the C=N bond of the pyrrole ring near 1389 cm^{-1}; the absorption peak at 1128 cm^{-1} was the skeleton vibration of the benzene ring, the –OH absorption peak was near 3387 cm^{-1}, the vibration peak of C=O was at 1675 cm^{-1}, and the characteristic peak of para-substitution of benzene ring was at 798 cm^{-1} [26, 27]. We propose that the mechanism was not simply an acid-base reaction because the FT-IR spectra showed that the hydrophilic EDA and –COOH group were not coordinated because the –OH peak was still observed, which indirectly demonstrated the stability of the material and the accuracy of detection. When the TCPP film was exposed to EDA, the stretching vibration of C=O at 1684 cm^{-1} became wider and even moved towards the direction of lower wavenumber [28], which indicated that a hydrogen bond formed between EDA and TCPP. In view of these facts, it is the formation of a strong hydrogen bond that results in the transfer of protons.

Conclusions. In summary, we have successfully prepared a TCPP film by spin coating, which has the merit of being a simple and highly efficient method without the need for toxic reagents. Moreover, we detected 18 kinds of VOC, and the sensor exhibited a highly selective response toward EDA gas and a low detection of 0.1 ppm (S/N = 5.05). The response and recovery times were 5 and 10 s, respectively. The results showed a significant relationship between the concentration of gas and the standard deviation with $R^2 = 0.9850$ and RSD = 6.25% in five parallel experiments. Additionally, the TCPP sensor exhibited good stability, repeatability, and reproducibility. In future studies, we expect to further show that this sensitive material has numerous applications for detecting EDA gas.

Acknowledgments. This work was supported by the National Natural Science Foundation of China (Grant No. 21765021). We thank Liwen Bianji, Edanz Group China (www.liwenbianji.cn/ac) for editing the English text of a draft of this manuscript.

REFERENCES

1. H. C. Liao, C. P. Hsu, M. C. Wu, C. F. Lu, and W. F. Su, *Anal. Chem.*, **85**, 9305–9311 (2013).
2. D. R. Kauffman and A. Star, *Angew. Chem. Int. Ed. Engl.*, **47**, 6550–6570 (2008).
3. C. H. Lv, L. B. Lv, and M. S. Chen, *J. Qiqihar Med. College*, **2001**, 88–89 (2001).
4. Y. L. Wang, Y. F. Xing, M. Yang, and Y. Mu, *Chin. Sanit. Eng.*, **2**, 104–106 (2014).
5. W. G. Tan, H. Z. Sun, J. Yang, and H. Wan, *Chin. Sanit. Eng.*, **2**, 32–36 (2012).
6. G. Li, X. Wang, T. Chen , M. Yang, Z. Zhang, T. Wu, and H. Chen, *Nano Lett.*, **8**, 2643–2647 (2008).
7. J. Roales, J. M. Pedrosa, P. Castillero, M. Cano, T. H. Richardson, A. Barranco, and A. R. Gonzalez-Elipe, *ACS Appl. Mater. Interfaces*, **4**, 5147–5154 (2012).
8. M. Imran, M. Ramzan, A. K. Qureshi, M. A. Khan, and M. Tariq, *Biosensors*, **8**, 95 (2018).
9. S. Kubendhiran, S. Sakthinathan, S. M. Chen, P. Tamizhdurai, K. Shanthi, and C. Karuppiah, *J. Colloid Interface Sci.*, **497**, 207–216 (2017).
10. P. Muthukumar and S. A. John, *Sens. Actuat. B*, **174**, 74–80 (2012).
11. G. Tuerdi, P. Nizamidin, N. Kari, A. Yimit, and F. Wang, *RSC Adv.*, **8**, 5614–5621 (2018).
12. H. Abudukeremu, N. Kari, Z. Yuan, J. Wang, P. Nizamidin, S. Abliz, and A. Yimit, *J. Mater. Sci.*, **53**, 1–13 (2018).
13. J. Denise, G. Favetto, S. Resnik, and J.Chirife, *J. Food Sci.*, **51**, 1037–1041 (1986).
14. W. Chen, F. Deng, M. Xu, J. Wang, Z. Wei, and Y. Wang, *Sens. Actuat. B*, **273**, 498–504 (2018).
15. R. Kadir, A. Yimit, H. Ablat, M. Mahmut, and K. Itoh, *Environ. Sci. Technol.*, **43**, 5113–5116 (2009).
16. E. S. Da Silva, N. M. M. Moura, M. G. P. M. S. Neves, A. Coutinho, M. Prieto, C. G. Silva, and J. L. Faria, *Appl. Catal. B*, **221**, 56–69 (2018).
17. R. J. Ma, L. Z. Zhao, J. B. Li, Y. Li, Y. L. An, L. and Q. Shi, *Biomacromolecules*, **9**, 2601–2608 (2008).
18. R. Bera, S. Mandal, B. Mondal, B. Jana, S. K. Nayak, and A. Patra, *ACS Sustain. Chem. Eng.*, **4**, 1562–1568 (2008).
19. P. Nizamidin, Y. Yan, G. Turdi, and A. Yimit, *Anal. Lett.*, **51**, 1–11 (2018).
20. M. Zhu, N. Kari, Y. Yan, and A. Yimit, *Anal. Methods*, **9**, 5494–5501 (2017).
21. J. R. Askim, M. Mahmoudi, and K. S. Suslick, *Chem. Soc. Rev.*, **42**, 8649–8682 (2013).
22. G. Tuerdi, N. Kari, Y. Yan, P. Nizamidin, and A. Yimit, *Sensors*, **17**, 2717 (2017).
23. N. Mataga, Y. Torihashi, and Y. Torihashi, *Theor. Chem. Acc.*, **2**, 168–176 (1964).

24. D. Kuciauskas and J. L. Humphrey, *J. Am. Chem. Soc.*, **128**, 3902–3903 (2006).
25. T. Yimamumaimaiti, S. Kuximake, P. Nizamidin, M. Mamuti, X. Abliz, and A. Yimit, *J. Sens. Technol.*, **1**, 8–12 (2019).
26. K. Q. Wang, H. X. Yang, and Q. F. Zhu, *J. Changchun Univ. Eng. (Nat. Sci. Ed.)*, **15**, 5–8 (2014).
27. L. L. Qin and Y. Yan, *Guangdong Chem. Ind.*, **9**, 21–22 (2013).
28. X. Y. Guo, P. Li, H. S. Shi, B. Zhang, Z. Q. Mao, and W. Q. Yao, *Polyurethane Ind.*, **4**, 9–12 (2016).